Modeling of Flexible and Rigid Wheels for Exploration Rover on Rough Terrain

Genya Ishigami[1)], Masatsugu Otsuki[1)], Takashi Kubota[1)], and Karl Iagnemma[2)]

[1)] *Institute of Space and Astronautical Science, Japan Aerospace Exploration Agency, Sagamihara, Japan*
[2)] *Department of Mechanical Engineering, Massachusetts Institute of Technology, U.S.A.*

This paper presents a comprehensive wheel model that can quantitatively evaluate traction performance of flexible/rigid wheels driving on deformable terrain. The proposed model exploits a terramechanics-based approach with taking account of pressures generated by wheel elasticity as well as terrain stiffness. Deflection of a flexible wheel typically depends on a relative pressure between the wheel and terrain: the wheel will be significantly deformed on rigid terrain whereas it will be hardly deformed on soft terrain. Therefore, the wheel-terrain interaction in the proposed model is divided into three contact sections: wheel front section, wheel deflected (flat) section, and wheel rear section. The traction force of the wheel is obtained as an integral of normal and shear stresses generated at each section. Simulation studies with varied wheel pressures, such as flexible, semi-flexible, and rigid wheels, are conducted to validate the proposed model. Also, traction performances of flexible/rigid wheels are compared based on a metric called tractive efficiency. The comparison implies an optimal wheel pressure of flexible wheel for better traction performance.

Key Words: Planetary Exploration Rover, Flexible wheel, Wheel contact model, and Terramechanics

1. Introduction

Wheeled mobility system has been utilized in lunar/planetary surface exploration because of its mechanical simplicity and maneuverability on rough terrain. Several types of wheels have been used for the mobility system for the surface exploration. The lunar roving vehicle in NASA's Apollo program employed flexible wheels with wire mesh carcass [1)]. The mars surface exploration rovers, such as Sojourner, MER rovers, and Curiosity have metallic rigid wheels with multiple grousers. The wheel of the ATHLETE has a performance similar to a pneumatic tire with the use of flexible spokes and a sheer band [2)]. The ExoMars rover in the European Space Agency will utilize flexible wheel with sheet metal [3)].

The mechanics of the interaction between wheel and terrain has been studied in *terramechanics* and there have been many researches devoted to the wheel-terrain interaction. A fundamental aspect of terramechanics was described in [4)], and also, the wheel traction performance with considering stress distribution has been investigated in [5)]. The terramechanic approach has been applied to the mobility analysis of lunar/planetary rovers: simplified wheel stress model and traction control methods have been developed in [6)]. A wheel contact model in steering motion has been proposed in [7)]. Also, wheel performances on deformable soil have been experimentally characterized [8)]. A rigid wheel mobility under low gravity condition has been tested in [9)].

The models developed in the above works have been well developed and experimentally validated; however, an explicit model that can address both flexible and rigid wheels on deformable terrain has not been well studied. Some resent works have been devoted to Discrete Element Method (DEM) for the wheel traction analysis on deformable terrain [10)−12)]. DEM approach is relatively useful for an analysis of flexible wheel on deformable terrain, however, it may require high computational effort since the model for wheel and terrain consist of vast number of elements.

In this paper, a wheel model that can evaluate the traction performance of both flexible and rigid wheels is presented. The proposed model simultaneously calculates a wheel deflection and a wheel sinkage based on a relationship between wheel pressure due to wheel structural stiffness and terrain pressure due to soil stiffness. The wheel model considers a wheel-terrain contact patch as three consecutive sections: wheel front section, wheel deflected (flat) section, and wheel rear section. Stress distribution at each section is formulated as a function of soil parameters, wheel traveling parameters, and wheel pressure due to wheel structural stiffness. The traction forces are then calculated by the normal and shear stresses generated at these three sections. Based on this approach, the proposed model can comprehensively address the both flexible and rigid wheels.

Simulation studies using the proposed model are described in this paper. The traction performances between flexible, semi-flexible, and rigid wheels are evaluated based on wheel sinkage, drawbar pull, resistance torque and tractive efficiency.

This paper is organized as follows: Section 2 introduces typical categories of wheel-terrain interaction mechanics and also describes assumptions in this work. Section 3 formulates the proposed model for flexible and rigid wheels. Section 4 presents the simulation studies.

2. Wheel-Terrain Interaction Category

In this paper, wheel-terrain interaction mechanics is categorized into four cases (Fig. 1). These categories are distinguished in accordance with the wheel pressure P_{wheel} due to wheel structural stiffness and terrain pressure $P_{terrain}$ by soil stiffness. The interaction in Category (a) may include a tribological property which is mainly composed of pure frictional relationship between wheel and terrain. An interaction of a conventional pneumatic tire traveling on road is categorized in (b), which has been significantly investigated as in [13)]. Therefore, the wheel model proposed in this paper

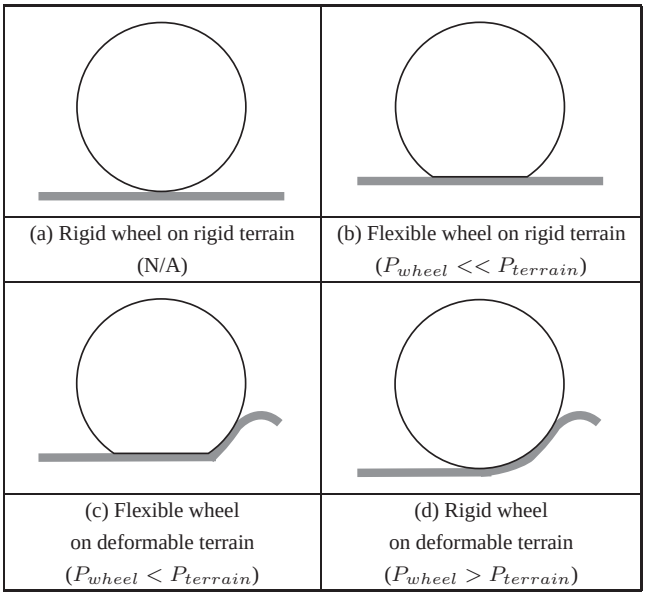

(a) Rigid wheel on rigid terrain (N/A)	(b) Flexible wheel on rigid terrain ($P_{wheel} << P_{terrain}$)
(c) Flexible wheel on deformable terrain ($P_{wheel} < P_{terrain}$)	(d) Rigid wheel on deformable terrain ($P_{wheel} > P_{terrain}$)

Fig. 1. Four categories for wheel-terrain interaction

aims to "seamlessly" cover the categories (c) and (d) with taking account of the relationship between the wheel pressure and terrain pressure.

The model developed in this paper considers the following three assumptions: The first assumption is that the deflected area of a flexible wheel is horizontally flat (Section BC in Fig. 2) and the normal stress beneath the flat section is uniformly distributed; The second assumption is that the contact patch of non-deformable sections, Section AB (front section) and Section CD (rear section) in Fig. 2, are circular arc; and, the third assumption is that the normal stress in the tire width direction is evenly distributed.

Note that, the first assumption for uniform distribution of normal stress has been experimentally confirmed in [14].

3. Interaction Model for Flexible and Rigid Wheels

First, the model developed in this paper calculates a static wheel sinkage (pure sinkage due to wheel load) and a wheel deflection based on a pressure relationship between wheel and terrain. Subsequently, a stress distribution at contact patches for driving wheel is formulated. Finally, wheel forces and torques can be obtained.

3.1 Static sinkage and wheel deflection

In static state (zero wheel velocity), a force balance in the vertical direction is the key to find a wheel sinkage and a wheel deflection. Assuming that a wheel having a certain amount of deflection δ_t and wheel static sinkage z_0 (Fig. 2) in a static state, a vertical reaction force F_{z0} is generated, which balances with the wheel load W. F_{z0} is given as a summation of the force generated at the non-deformed section AB and CD ($= 2F_s$) and the other force at the flat section BC ($= F_w$):

$$F_{z0} = F_w + 2F_s \tag{1}$$

where $F_w = P_w b l_t$ as P_w is the wheel pressure due to the wheel structural stiffness, b is the wheel width, and l_t is the

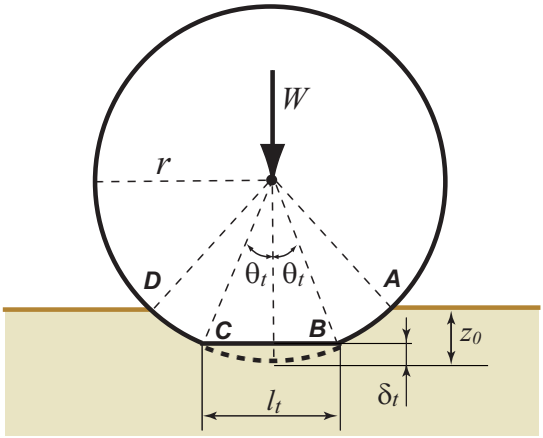

Fig. 2. Wheel-terrain model at static state

horizontal length of the wheel flat section. Also, F_s is obtained by the following equation:

$$F_s = \left[b(k_c/l_t) + k_\phi\sqrt{D}(z_0+\delta_t)^{n-1}\right] \times \frac{(3-n)[(z_0+\delta_t)^{3/2} - \delta_t^{3/2}] - 3z_0\sqrt{\delta_t}}{3} \tag{2}$$

D is the wheel diameter and k_c and k_ϕ represent the soil-dependent parameter for pressure-sinkage moduli.

The equation above indicates that the vertical reaction force of a wheel at static state is given as a function of δ_t, l_t, and z_0. The length of the wheel flat section and the wheel sinkage are respectively calculated as follows:

$$l_t = 2\sqrt{D\delta_t - \delta_t^2} \tag{3}$$

$$z_0 = \begin{cases} \left(\frac{P_w}{k_c/l_t + k_\phi}\right)^{1/n} & (\text{if } \ l_t < b) \\ \left(\frac{P_w}{k_c/b + k_\phi}\right)^{1/n} & (\text{if } \ l_t \geq b) \end{cases} \tag{4}$$

where n is the sinkage exponent.

The wheel deflection δ_t can be found through an iterative procedure. In the iteration process, first, an initial value for δ_t is given which is substituted into Eq. (3) to calculate l_t. Then, the wheel sinkage is obtained by Eq. (4). The vertical force F_{z0} with the given parameter sets can be calculated by (1). If F_{z0} is equal to the vertical load W, the value of δ_t is correctly determined. If not, different value for δ_t is given again and the above procedure is repeated until the correct δ_t is found.

Note that, in the analysis described in this paper, the bisection method is employed to let δ_t converge within an appropriate value; if the angle θ_t (angle between the vertical and the point where the wheel deflection initiates) is less than 0.5 degrees, the wheel is assumed as a rigid enough relative to terrain pressure.

3.2 Normal stress ans shear stress distribution

Fig. 3 illustrates a normal stress distribution beneath a driving wheel. In this work, the normal stress at the front and rear section (σ_f and σ_r) are obtained based on the

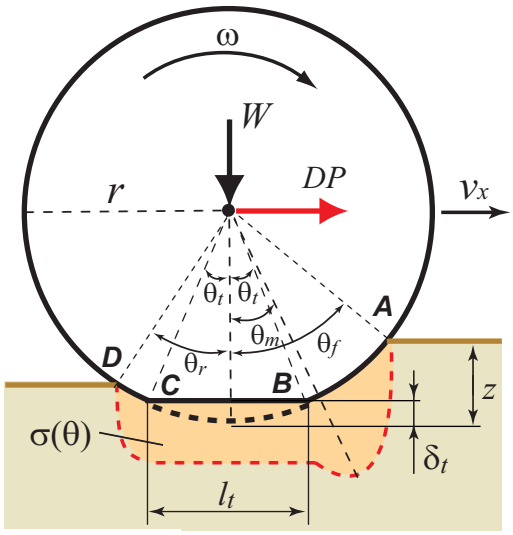

Fig. 3. Wheel-terrain model: Normal stress distribution of driving wheel

model proposed in [5]. The normal stress at the flat section σ_t is assumed as uniformly distributed along with the soil-dependent parameters:

$$\sigma(\theta) = \begin{cases} \sigma_f = \sigma_m(\cos\theta - \cos\theta_f)^n \\ \sigma_t = \begin{cases} (k_c/l_t + k_\phi)(z-\delta_t)^n & (\text{if } \ l_t < b) \\ (k_c/b + k_\phi)(z-\delta_t)^n & (\text{if } \ l_t \geq b) \end{cases} \\ \sigma_r = \sigma_m \left\{ \cos\left[\theta_f - \frac{(\theta-\theta_r)(\theta_f-\theta_m)}{(\theta_m-\theta_r)}\right] \cos\theta_f \right\}^n \end{cases} \tag{5}$$

where $\sigma_m = r^n(k_c/b + k_\phi)$, r is the wheel radius. θ_f and θ_r are the entry and exit angles of the wheel contact patch, respectively calculated as:

$$\theta_f = \cos^{-1}(1 - z/r) \tag{6}$$

$$\theta_r = \cos^{-1}(1 - \lambda z/r) \tag{7}$$

z is the wheel sinkage and λ indicates the terrain reboundness due to soil elasticity.

Also, θ_m is the angle at which the normal stress has a maximum, defined as [15]:

$$\theta_m = (a_0 + a_1 s)\theta_f \tag{8}$$

where a_0 and a_1 are parameters that depend on the wheel-soil interaction. These values are generally assumed as $a_0 \approx 0.4$ and $0 \leq a_1 \leq 0.3$. s is the slip ratio of wheel (i.e. slip in the longitudinal direction of wheel travel), defined as a function of the longitudinal traveling velocity of the wheel v_x and the circumferential velocity of the wheel $r\omega$:

$$s = \begin{cases} (r\omega - v_x)/r\omega & (|r\omega| \geq |v_x| : \text{driving}) \\ (r\omega - v_x)/v_x & (|r\omega| < |v_x| : \text{braking}) \end{cases} \tag{9}$$

The slip ratio assumes a value in the range from -1 to 1.

Table 1 summarizes the applicable equations from Eq. (5) in accordance with the wheel contact angle θ.

During a wheel driving, a shear deformation of soil beneath the wheel is generated. The shear stress $\tau(\theta)$ is obtained by the following equation [16]:

$$\tau(\theta) = [c + \sigma(\theta)\tan\phi][1 - e^{-j(\theta)/k}] \tag{10}$$

Table 1. Applicable equations for normal stress at each contact section

$\sigma(\theta)$	if $\theta_m > \theta_t$	if $\theta_m \leq \theta_t$
σ_f	$\theta_m \leq \theta \leq \theta_f$	$\theta_t \leq \theta \leq \theta_f$
σ_t	$-\theta_t \leq \theta < \theta_t$	$-\theta_t \leq \theta < \theta_t$
σ_r	$\theta_t \leq \theta < \theta_m$ $\theta_r \leq \theta < -\theta_t$	$\theta_r \leq \theta < -\theta_t$

where c is the soil cohesion, ϕ is the internal friction angle of soil, and k is the shear deformation modulus. The soil deformation $j(\theta)$ for the front and rear sections is given as a function of slip ratio and contact angle [15]:

$$j(\theta) = r\left[\theta_f - \theta - (1-s)(\sin\theta_f - \sin\theta)\right] \quad (\text{if } \ |\theta| \geq |\theta_t|) \tag{11}$$

The shear deformation at the flat section is equivalent with the relative displacement from the angle at which the wheel initially deflects, which is modeled in this paper as:

$$j(\theta) = j(\theta_t) + s(r\sin\theta_t - (r - \delta_t)\tan\theta) \quad (\text{if } \ |\theta| < |\theta_t|) \tag{12}$$

3.3 Wheel force

The wheel-terrain interaction model proposed in this paper calculates wheel forces as a summation of forces generated at each section of wheel contact patch. These forces are obtained by integrating the normal and shear stresses modeld in Section 3.2.

The vertical force F_z for the driving wheel is modeled as:

$$\begin{aligned} F_z = \ & rb\int_{\theta_t}^{\theta_f}\{\tau(\theta)\sin\theta + \sigma(\theta)\cos\theta\}d\theta \\ & + \sigma_t b l_t \\ & + rb\int_{\theta_r}^{-\theta_t}\{\tau(\theta)\sin\theta + \sigma(\theta)\cos\theta\}d\theta \end{aligned} \tag{13}$$

The first and third terms of the above equation are the vertical forces generated at front and rear sections, and the second term is the one at the flat section.

The thrust force H of the wheel can be given by the following equation:

$$\begin{aligned} H = \ & rb\int_{\theta_t}^{\theta_f}\tau(\theta)\cos\theta d\theta \\ & + (r - \delta_t)b\int_{-\theta_t}^{\theta_t}\tau(\theta)/\cos^2\theta d\theta \\ & + rb\int_{\theta_r}^{-\theta_t}\{\tau(\theta)\cos\theta - \sigma(\theta)\sin\theta\}d\theta \end{aligned} \tag{14}$$

The resistance force R is also obtained as a summation of a resistance due to soil compaction in the front section and another resistance due to the wheel deflection (or wheel flexing resistance):

$$R = rb\int_{\theta_t}^{\theta_f}\sigma(\theta)\sin\theta d\theta + R_w \tag{15}$$

The resistance force due to the wheel deflection has been experimentally modeled by several approaches. For example, it is modeled as a function of wheel load, wheel pressure, and wheel structural parameters [4][17]. In this paper, the following equation developed by [5] is employed since it includes parameters for wheel deflection:

$$R_w = \left[3.581 b D^2 P_w \epsilon(0.0349\theta_t - \sin 2\theta_t)\right] / (\theta_t(D^2 - \delta_t)) \tag{16}$$

Table 2. Simulation parameters and values

Parameter	Value	Unit
c	800.0	Pa
ϕ	37.2	deg
k_c	1.37×10^3	N/m^{n+1}
k_ϕ	8.14×10^5	N/m^{n+2}
n	1.0	-
k	0.02	m
λ	0.1	-
a_0	0.4	-
a_1	0.15	-
k_e	7.0	-
h	0.05	m
W	5.0	kg
D	0.20	m
b	0.10	m
P_w	1250, 2500, 5000, 10000	Pa

where $\epsilon = 1 - \exp(-k_e \delta_t / h)$ as h is the deformable section height of the wheel and k_e is a parameter related to wheel construction. The unit of θ_t is in degrees in the above equation. The values for k_e is assumed as 7 as noted in [5]. Note that Eq. (16) needs to be experimentally re-determined since it has been developed for the use of a pneumatic tire. The simulation study described below includes Eq. (16) as an offset resistance for flexible wheels.

Finally, the net traction force called drawbar pull is obtained as the difference between the thrust and the resistance force:

$$DP = H - R \tag{17}$$

3.4 Tractive Efficiency

The tractive efficiency is used to characterize the efficiency of the wheel in transforming the input power (torque required for wheel driving) to the output power available at the drawbar (net traction force). The tractive efficiency is defined as the ratio of the output power to the input power:

$$\eta = \frac{DP \cdot v_x}{T\omega} = \frac{DP(1-s)r}{T} \tag{18}$$

where T is the input torque to the driving axle. In the steady state, the driving torque should be equivalent to the resistance torque. The resistance torque is given as a summation of the shear stress generated around the circumference of the wheel:

$$\begin{aligned} T = \; & r^2 b \int_{\theta_t}^{\theta_f} \tau(\theta) d\theta \\ & + (r - \delta_t)^2 b \int_{-\theta_t}^{\theta_t} \{\tau(\theta) + \sigma_t \tan\theta\} / \cos^2\theta d\theta \\ & + r^2 b \int_{\theta_r}^{-\theta_t} \tau(\theta) d\theta \end{aligned} \tag{19}$$

4. Simulation Study for Flexible/Rigid wheels

Simulation studies using the wheel model described in Section 3 are conducted. In the simulation study, the traction performances between flexible/rigid wheels with varied wheel pressures are evaluated based on wheel sinkage, drawbar pull, resistance torque, and tractive efficiency.

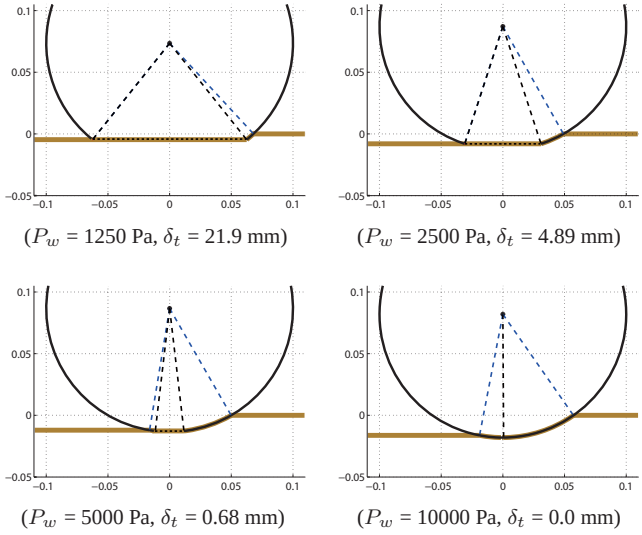

Fig. 4. Wheel deflection and contact patch with varied wheel pressures

4.1 Simulation condition

Wheels tested in the simulation are set with four different values of wheel pressures as P_w is respectively given as 1250, 2500, 5000, and 10000 Pa. The diameter of the test wheel is set as 0.2 m, and the width is 0.1 m. The wheel load is given as 5.0 kg. The parameters used in the simulation are listed in Table 2.

The procedure for the numerical simulation is summarized as follows:

1. input the wheel load W and slip ratio s
2. find the wheel deflection δ_t at static state by the procedure described in Section 3.1
3. calculate the wheel sinkage at the kinetic state (driven wheel) from the relationship between W and F_z as defined in Eq. (13):
   (a) input the initial value for wheel sinkage (i.e. z_0)
   (b) calculate the wheel contact patch (entry angle and exit angle)
   (c) determine the normal stress and the shear stress by Eq. (5) and Eq. (10), and then, calculate the vertical force F_z by Eq. (13)
   (d) if $W \neq F_z$, return to Step 3-a) with an increase of wheel sinkage. If $W = F_z$, proceed to the following steps.
4. calculate the thrust, the resistance force, the drawbar pull by Eqs. (14), (15), and (17)
5. calculate the tractive efficiency by Eq. (18).

The above calculation steps for each wheel are carried out with varied slip ratio, which is set from 0.0 to 1.0 in steps of 0.05.

4.2 Simulation resutls and discussions

4.2.1 Wheel deflection and sinkage

Fig. 4 and Fig. 5 show the simulation results for the wheel deflection and sinkage. From the graphs, first, the wheel deflection increases as the wheel pressure decreases, and also,

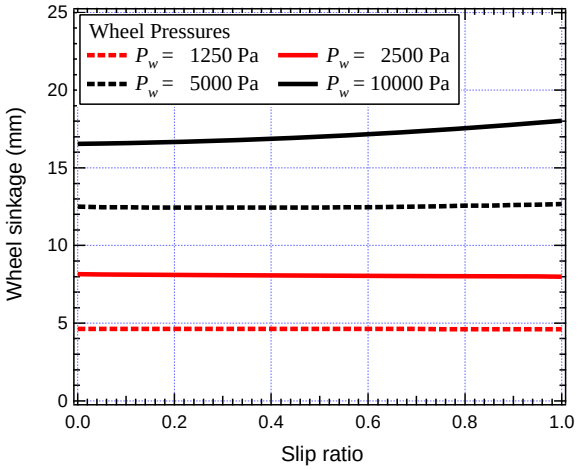

Fig. 5. Wheel sinkage with varied wheel pressure

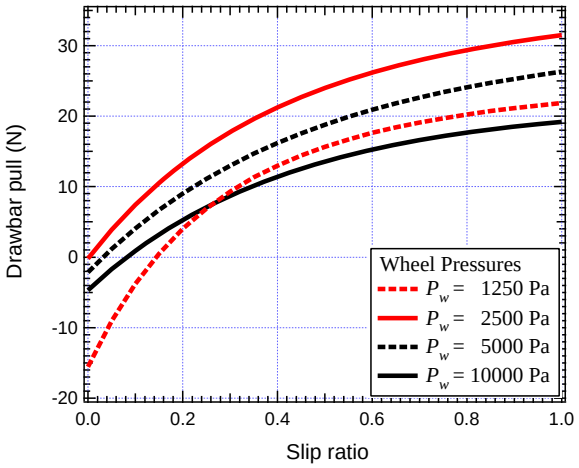

Fig. 6. Drawbar pull with varied wheel pressure

the wheel sinkage decreases with decreasing the wheel pressure. This is because low wheel pressure easily deflects the wheel shape which generates larger flat section of wheel, resulting in less wheel sinkage. The wheel having P_w=10000 Pa can be assumed as "rigid wheel" since its deflection is 0 mm, while others are "flexible wheels".

From Fig. 5, the wheel sinkage of the most rigid wheel (black line) increases as the slip ratio increases. This is due to the fact that the shear deformation of wheel increases with increasing the slip ratio. However, the sinkage of the other wheels are almost constant regardless of slip ratio since the flat section of the wheel mostly supports the vertical load of wheel.

These results confirm that the proposed model can appropriately calculate wheel deflection/sinkage in accordance with the wheel pressures.

4.2.2 *Drawbar pull*

The simulation result for the drawbar pull with varied wheel pressure is shown in Fig. 6. The drawbar pull increases as the slip ratio increases regardless of the wheel pressure.

It can be seen that the wheel with the lowest wheel pressure generates relatively small drawbar pull, in particular, the drawbar pull at low slip ratio takes significantly negative

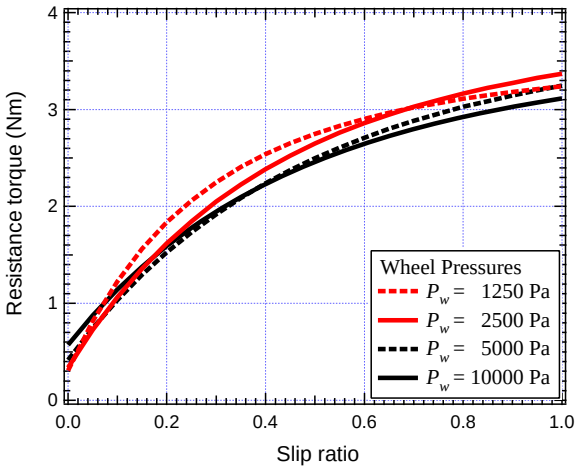

Fig. 7. Resistance torque with varied wheel pressure

value. This is attributable to the resistance force due to the wheel deflection that is calculated around -20 N.

On the other hand, the wheels with $P_w = 2500$ and $P_w = 5000$ Pa generate positive drawbar pull regardless of slip ratio. This is explained in terms of the force generated at the flat section of the wheel. The shearing direction at the flat section is parallel to the direction of wheel traveling, resulting in the increase of the thrust. In addition, the resistance force due to the wheel deflection is not notable for these semi-flexible wheels. Therefore, the gross net traction becomes large as compared to the rigid wheel or the wheel with P_w =1250 Pa.

It should be emphasized that the wheel with P_w =2500 Pa has a maximum drawbar pull in every slip ratio as compared to the other wheels even though the pressure of the wheel is moderate one between the four wheels. This result implies that an optimal wheel pressure for drawbar performance may exist.

4.2.3 *Resistance torque*

The proposed model also derives the characteristics of the resistance torque of the wheels, as shown in Fig. 7. The resistance torque of the rigid wheel (P_w =10000 Pa) is the lowest in slip ratio of over 0.3. The other flexible wheel (P_w =1250 and 2500 Pa) generates relatively high resistance torque owing to the shear and normal stress at flat section. From the findings at the drawbar pull and the resistance torque, the flat section of the wheel contributes an increase of the drawbar pull but also requires an increase of the input torque to the wheel.

4.2.4 *Tractive efficiency*

Fig. 8 shows the simulation results for the tractive efficiency with varied wheel pressures. From the graph, one of the important findings is that the tractive efficiency has a maximum curve at $P_w = 2500$ Pa at every slip ratio. This is because the drawbar pull of the wheel is positive regardless of the slip ratio and the resistance torque of the wheel is not significant as compared to the other wheels. This result confirms that an optimal wheel pressure for better traction performance certainly exists. Comparing the wheels with $P_w = 1250$ and 10000 Pa, the characteristics curves for the

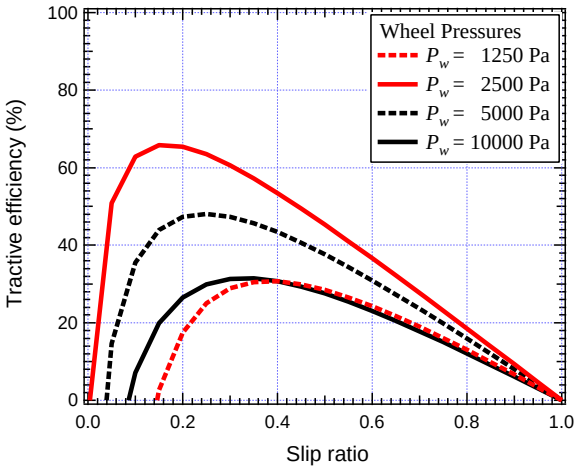

Fig. 8. Tractive efficiency with varied wheel pressure

tractive efficiency are almost equivalent: the peak value is about η =30 % at slip ratio of around 0.3 $\sim$ 0.4. This characteristic implies that a flexible wheel having too low wheel pressure does not show good performance for rough terrain travel.

4.2.5 Summary

From the results and discussions, the wheel traction characteristics are determined by the relationship between the drawbar pull and the resistance torque: a rigid wheel has small drawbar pull as well as small resistance torque, whereas a flexible wheel large drawbar requiring large resistance torque. An optimal wheel pressure can be found based on a wheel load, terrain stiffness, and wheel structure.

In this work, the values for the wheel parameters such as k_e and h are given based on previous works, however, the results are qualitatively reasonable for a discussion of the tractive performance of flexible/rigid wheels. Therefore, it can be stated that the proposed model can comprehensively address both flexible/rigid wheel along with its varying wheel pressure.

5. Conclusion

In this paper, a comprehensive wheel model that can analyze the traction performance of both flexible and rigid wheel has been developed. The proposed model considers a relationship of pressures between wheel and terrain at the contact patch: a wheel deflection and wheel sinkage are simultaneously obtained based on the relationship of wheel pressure due to wheel structural stiffness and terrain pressure due to soil stiffness. The stress distributions at the contact patch is divided into three sections, wheel front section, wheel flat section, and wheel rear section, and then, the wheel forces are calculated based on the normal and shear stress.

Simulation studies have confirmed that the wheel model developed in this paper can properly analyze both flexible and rigid wheel performances. In particular, the simulation results have indicated that an optimal wheel pressure is determined based on a wheel load, wheel dimension, and terrain stiffness.

Future direction of this work includes an experimental validation of the proposed model. In addition, parameter identification for wheel structural property will be necessary for the comparison between theoretical and experimental results.

References

1) V. Asnani, D. Delap, and C. Creager, "The development of wheels for the Lunar Roving Vehicle," *J. of Terramechanics*, vol. 46 pp. 89-103, 2009.
2) B. H. Wilcox, T. Litwin, J. Biesiadecki, J. Matthews, M. Heverly, J. Morrison, J. Townsend, N. Ahmad, A. Sirota, and B. Cooper, "Athlete: A cargo handling and manipulation robot for the moon," *J. of Field Robotics*, vol. 24, pp. 421-434 ,2007.
3) N. Patel, R. Slade, and J. Clemmet, "The ExoMars rover locomotion subsystem," *J. of Terramechanics*, vol. 47, pp. 227-242, 2010.
4) M. Bekker, *Off-The-Road Locomotion*, The University of Michigan Press, 1960.
5) J. Wong, *Theory of Ground Vehicles*. 4th Ed., New York, Wiley, 2008.
6) K. Iagnemma and S. Dubowsky, *Mobile Robots in Rough Terrain: Estimation, Motion Planning, and Control with Application to Planetary Rovers*, Springer Tracts in Advanced Robotics, 2004.
7) G. Ishigami, A. Miwa, K. Nagatani, and K. Yoshida, "Terramechanics-Based Model for Steering Maneuver of Planetary Exploration Rovers on Loose Soil," *J. of Field Robotics*, vol. 24, no. 3, pp. 233-250, 2007.
8) L. Ding, H. Gao, Z. Deng, K. Nagatani, and K. Yoshida, "Experimental study and analysis on driving wheels' performance for planetary exploration rovers moving in deformable soil," *J. of Terramechanics*, vol. 48, pp. 27-45, 2011.
9) T. Kobayashi, Y. Fujiwara, J. Yamakawa, N. Yasufuku, and K. Omine, "Mobility performance of a rigid wheel in low gravity environments," *J. of Terramechanics*, vol. 47, pp. 261-274, 2010.
10) H. Nakashima, H. Fujii, A. Oida, M. Momozu, Y. Kawase, H. Kanamori, S. Aoki, and T. Yokoyama, "Parametric analysis of lugged wheel performance for a lunar microrover by means of DEM," *J. of Terramechanics*, vol. 44, pp. 153-162, 2007.
11) H. Nakashima, H. Fujii, A. Oida, M. Momozu, H. Kanamori, S. Aoki, T. Yokoyama, H. Shimizu, J. Miyasaka, and K. Ohdoi, "Discrete element method analysis of single wheel performance for a small lunar rover on sloped terrain," *J. of Terramechanics*, vol. 47, pp. 307-321, 2010.
12) W. Li, Y. Huang, Y. Cui, S. Dong, and J. Wang, "Trafficability analysis of lunar mare terrain by means of the discrete element method for wheeled rover locomotion," *J. of Terramechanics*, vol. 47, pp. 161-172, 2010.
13) H. B. Pacejka, *Tyre and Vehicle Dynamics*, Butterworth-Heinemann, Oxford, 2002.
14) S. Narita, M. Otsuki, S. Wakabayashi, and S. Nishida, "Terramechanics Evaluation of Low-Pressure Wheel on Deformable Terrain," in *Proc. of the 2011 IEEE Int. Conf. on Robotics and Automation*, Shanghi, China, (accepted).
15) J. Wong and A. Reece, "Prediction of Rigid Wheel Prefoemance Based on the Analysis of Soil-Wheel Stresses Part I, Preformance of Driven Rigid Wheels," *J. of Terramechanics*, vol.4, pp. 81-98, 1967.
16) Z. Janosi and B. Hanamoto, "The analytical determination of drawbar pull as a function of slip for tracked vehicle," in *Proc. of the 1st Int. Conf. on Terrain-Vehicle Systems*, Torino, pp. 707-736, 1961.
17) G. Tiwari and K. Pandey, "Performance prediction of animal drawn vehicle tyres in sand," *J. of Terramechanics*, vol.45, pp. 193-200, 2008.